

Article

Temperature Dependence of the Number of Defect-Structures in Poly(vinylidene fluoride)

Jan Schwaderer, Marco Drache  and Sabine Beuermann * 

Institute of Technical Chemistry, Clausthal University of Technology, Arnold-Sommerfeld-Straße 4, 38678 Clausthal-Zellerfeld, Germany; jan.schwaderer@tu-clausthal.de (J.S.); marco.drache@tu-clausthal.de (M.D.)
* Correspondence: sabine.beuermann@tu-clausthal.de

Abstract: Poly(vinylidene fluoride) (PVDF) is predominantly characterized by alternating CH₂ and CF₂ units in a polymer backbone, originating from the head-to-tail addition of monomers or regular propagation. Due, to a small extent, to inverse monomer addition, so-called defect structures occur which influence the macroscopic properties of PVDF significantly. The amount of defect structures in the material is determined by the polymerization conditions. Here, the temperature dependence of the fraction of defect structures in PVDF obtained from polymerizations between 45 and 90 °C is reported. We utilized ¹⁹F-NMR spectroscopy to determine the fraction of defect structures as a function of temperature. To derive kinetic data, the polymerization of VDF is considered a quasicopolymerization described by the Terminal Model involving four different propagation reactions. Based on the experimentally determined temperature-dependent fractions of defect structures, the known overall propagation rate coefficient, and taking into account the self-healing behavior of the macroradical, the Arrhenius parameters of the individual propagation rate coefficients were determined using the Monte Carlo methods.

Keywords: PVDF; defect structure; temperature dependence



Citation: Schwaderer, J.; Drache, M.; Beuermann, S. Temperature Dependence of the Number of Defect-Structures in Poly(vinylidene fluoride). *Molecules* **2024**, *29*, 1551. <https://doi.org/10.3390/molecules29071551>

Academic Editors: Cyrille Boyer, Bruno Ameduri and Benoit Briou

Received: 2 March 2024

Revised: 25 March 2024

Accepted: 26 March 2024

Published: 29 March 2024

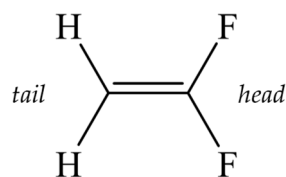


Copyright: © 2024 by the authors. Licensee MDPI, Basel, Switzerland. This article is an open access article distributed under the terms and conditions of the Creative Commons Attribution (CC BY) license (<https://creativecommons.org/licenses/by/4.0/>).

1. Introduction

Poly(vinylidene fluoride) (PVDF) is a thermoplastic fluoropolymer. It is characterized by high thermal stability and resistance to acids and UV radiation, as well as low flammability [1,2] and a degree of crystallinity between 35 and 70% [3]. Due to its exceptional properties, PVDF is used in a wide range of applications, including valves, pumps, paints, and insulation materials [1]. In addition, the crystalline fraction of PVDF can exist in five different polymorphic phases [4,5]. The β phase is particularly interesting, because it possesses a macroscopic dipole moment, thereby exhibiting piezoelectric, ferroelectric, and pyroelectric properties [5,6]. Thus, PVDF with a high β -phase content is of interest for electronic components, solar panels, and sensors [7,8]. Because of its unique spectrum of properties, PVDF is the second most used fluoropolymer [9].

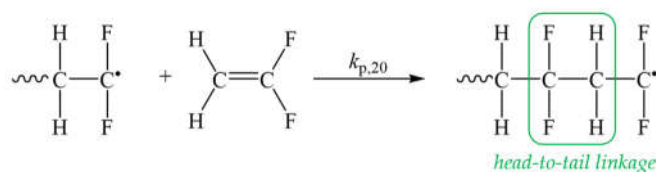
The microstructure of PVDF is described by its molar mass distribution, the degree of branching, and the proportion of defect structures. These structural characteristics are strongly influenced by the choice of process conditions for radical polymerization. For example, by employing controlled radical polymerization techniques, PVDF with narrow molar mass distributions (MMDs) and a small number of branch points is obtained [10,11], while free radical polymerizations lead to broader MMDs and a higher degree of branching. The polymer microstructure significantly impacts its properties, including the degree of crystallization [12], miscibility [13], and the type of polymorph formed [14,15]. This work deals with the influence of temperature on the fraction of defect structures. This structural motif originates from the fact that VDF is an asymmetric monomer that consists of a head (CF₂ group,) and a tail (CH₂ group), as shown in Scheme 1.



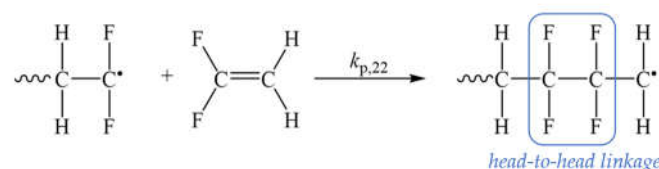
Scheme 1. Chemical structure of VDF.

Upon addition of a radical to the monomer, the radical functionality is preferably located at the CF_2 group. If the addition of the next VDF unit occurs in a manner that preserves the CF_2 radical functionality at the chain end, a head-to-tail linkage is formed. This propagation step is referred to as regular propagation of the PVDF macroradical and occurs preferentially during polymerization. This reaction leads to a polymer backbone consisting of alternating CF_2 and CH_2 groups, as illustrated in the upper part of Scheme 2. However, other propagation reactions are feasible, too. A change in radical functionality occurs if a macroradical with a terminal CF_2 group adds to the head side of the VDF molecule and a head-to-head linkage is created. This irregular addition of monomer leads to so-called defect structures $-\text{CF}_2-\text{CF}_2-$ in the polymer backbone (second reaction in Scheme 2). According to IUPAC recommendations, the terms regioregular and regioirregular are used for head-to-tail and head-to-head linkages, respectively [16]. Since the majority of all previous publications related to PVDF use the term “defect structure”, this term is used in the following. Defect contents between 5% and 10% were reported [3,16–21]. The fraction of defect structures influences the degree of crystallinity, toughness, mechanical strength, and impact resistance of PVDF [7]. In addition, to obtain high fractions of β -phase material the number of defect structures should be low [5,22].

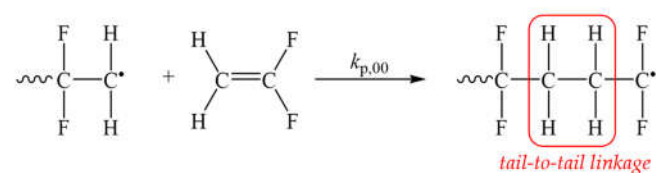
(a) Regular chain propagation reaction



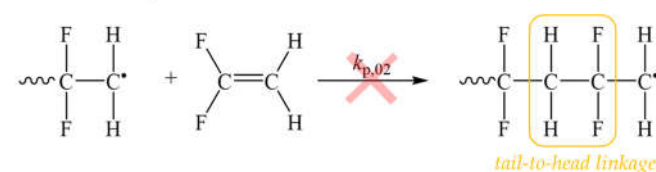
(b) Inverted monomer addition



(c) Self-healing of the PVDF chain



(d) tail-to-head growth does not occur



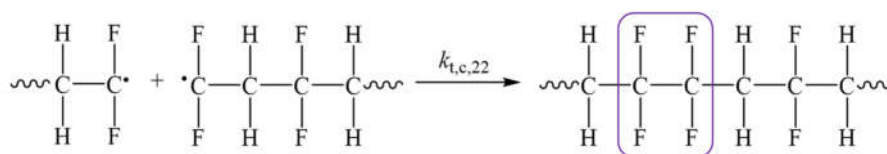
Scheme 2. The quasi-copolymerization of VDF is described by the regular and inverse incorporation of monomers via four distinct propagation reactions according to the terminal model.

Irregular propagation results in a terminal CH_2 radical functionality, which in turn enables two additional growth reactions. In the first case, the preferred CF_2 radical functionality is restored, resulting in a tail-to-tail linkage, as illustrated in part c of Scheme 2. This growth reaction is called defect healing and, in the case of free radical VDF polymerization, always follows irregular propagation [23]. This phenomenon is also referred to as self-healing of the PVDF chain. As a result, a tail-to-head linkage cannot be formed (see lower part of Scheme 2).

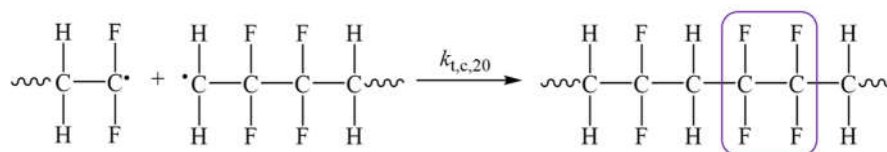
The following terminology is introduced for naming the carbon units. Each carbon atom is coded by a digit, where the digit value corresponds to the number of fluorine atoms directly attached to that carbon atom. Carbon atoms that do not carry fluorine atoms are abbreviated with the digit 0 (CH_2). Therefore, the number 2 represents a carbon atom with two directly bonded fluorine atoms (CF_2). These naming conventions result in the propagation coefficients $k_{p,20}$ for regular growth (head-to-tail growth), $k_{p,22}$ for defect growth (head-to-head-growth), $k_{p,00}$ for defect healing (tail-to-tail growth), and $k_{p,02}$ for tail-to-head growth, which, in this case, assumes a value of 0.

In the case of VDF polymerizations, termination occurs exclusively through combination [19,24], which suggests that, in principle, a relatively large fraction of the defect structure could arise from bimolecular termination, as illustrated in Scheme 3. The structural motif $-\text{CH}_2-\text{CF}_2-\text{CH}_2-\text{CF}_2-\text{CF}_2-\text{CH}_2-\text{CF}_2-\text{CH}_2-\text{CF}_2-$ formed via termination reactions (a) and (b) in Scheme 3, was not detected in the ^{19}F -NMR spectrum. The termination of two macroradicals with terminal CH_2 radical functionalities (termination reaction (c)) is unlikely since only a very small number of these species is present in the reaction mixture. For these reasons, in general, it is assumed that the contribution of termination to the fraction of CF_2-CF_2 structures is negligible.

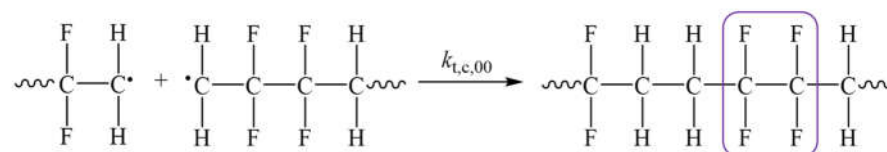
(a) Termination of two CF_2 -terminated macroradicals



(b) Termination of one CF_2 -terminated and one CH_2 -terminated macroradical



(c) Termination of two CH_2 -terminated macroradicals



Scheme 3. The defect structure $-\text{CF}_2-\text{CF}_2-$ can also result from termination by combination.

In the context of this work, PVDF which was obtained by a rather special type of polymerization known as pulsed laser-initiated polymerization (PLP) was analyzed [25,26]. Generally, PLP is characterized by the generation of initiator-derived radicals by applying an evenly-spaced sequence of short UV laser pulses to a mixture consisting of monomer and photoinitiator [27]. Additionally, a solvent undergoing little chain transfer may be present. Since a high concentration of initiator radicals, typically in the order of $10^{-6} \text{ L}\cdot\text{mol}^{-1}\cdot\text{s}^{-1}$, is generated at a certain moment in time, the probability of termination events at this moment

in time is significantly enhanced. Consequently, the termination of an initiator-derived radical and a macroradical is favored. The likelihood of a bimolecular chain termination reaction, where two growing chains combine, is significantly reduced [28]. Moreover, the probability of chain propagation is significantly higher than of chain termination due to the significantly higher monomer concentration compared to the radical concentration. Thus, as discussed for the general case of VDF radical polymerizations, for polymers obtained from PLP, termination as a source of $\text{CF}_2\text{-CF}_2$ defects is also negligible.

2. Results and Discussion

The fraction of defect structures in PVDF is calculated using ^{19}F -NMR spectroscopy. At a chemical shift of -91.4 ppm, the signal of regular PVDF growth is detected [29]. Three additional signals are observed, at -94.5 ppm, -113.8 ppm, and -116.2 ppm. These signals are assigned to the fluorine atoms of CF_2 groups located in the immediate vicinity of defect propagation [29]. In Figure 1, an exemplary ^{19}F -NMR spectrum and the associated structural motifs are shown. The orange marked signal at -113.8 ppm corresponds to the fluorine atoms of a CF_2 group to which the following VDF unit is inversely added. The blue signal at -116.2 ppm is assigned to the fluorine atoms of an inversely incorporated VDF unit. At a chemical shift of -94.5 ppm, the red-marked signal corresponds to a VDF unit directly following a defect growth. This VDF unit, obtained through a tail-to-tail linkage, is attributed to defect healing of the PVDF chain.

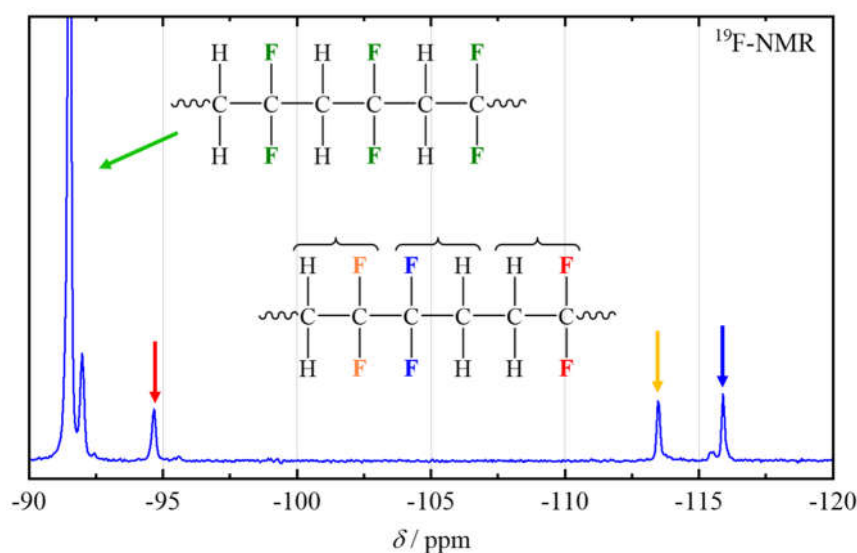


Figure 1. ^{19}F -NMR spectrum of a typical PVDF sample.

To determine the self-healing degree of PVDF, the integrals of the signals of the defect-causing VDF units and the defect-healing VDF units can be put into proportion, as shown in Equation (1). A_i denotes the integral of the respective signal at the chemical shift $\delta = i$ ppm in the ^{19}F -NMR spectrum.

$$\text{degree of self-healing} = \frac{A_{-116.2}}{A_{-94.5}} \quad (1)$$

In Figure 2, it is shown that the experimentally derived data for the degree of self-healing are predominantly between 1.0 and 1.1, with an average value of 1.02. The *degree of self-healing* does not show a systematic variation with polymerization conditions (temperature, pressure) and molecular weight. Since the ^{19}F -NMR spectra do not show any peaks that may be assigned to the above-mentioned termination products, the defect structures

are due to inverse monomer incorporation. The content of defect structures in PVDF is calculated using Equation (2).

$$\text{defect content}_{\text{exp}} = \frac{A_{-116.2}}{A_{-91.4} + A_{-94.5} + A_{-113.8} + A_{-116.2}} \times 100\% \quad (2)$$

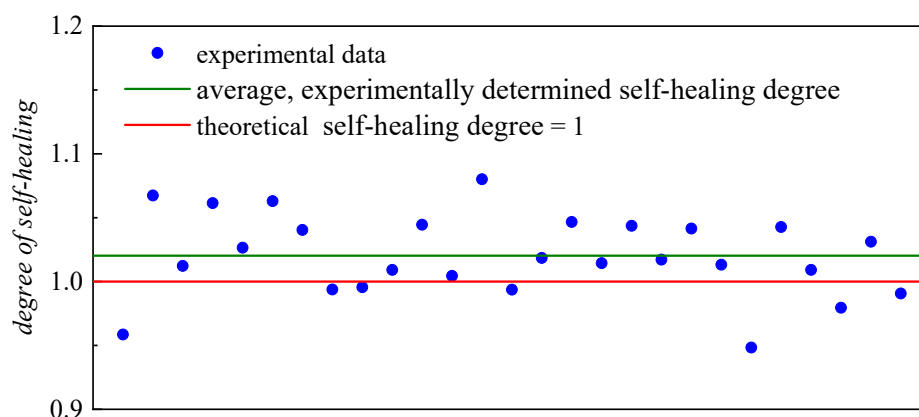


Figure 2. The degree of self-healing as determined experimentally and the average value of all individual data. The red line indicates the theoretical value of 1.

Upon valuation of all the NMR data, a temperature dependence on the number of defect structures in the PVDF became evident. With the increasing polymerization temperature, a higher fraction of defect structures were generated in the PVDF, which is in line with previous reports [22]. In order to tailor PVDF with respect to the number of defect structures via kinetic modeling, knowledge of the temperature dependence of all kinetic coefficients for the reactions shown in Scheme 2 is required. While these individual coefficients are not accessible from experiments, the overall polymerization propagation rate coefficient $k_{p,\text{app}}$ was already reported [25]. The values of $k_{p,\text{app}}$ are related to the individual coefficients $k_{p,20}$, $k_{p,22}$, $k_{p,00}$, and $k_{p,02}$ using Equation (3), which was derived for the quantification of defect structures in poly(vinyl acetate) [30].

$$k_{p,\text{app}} = k_{p,20} - \frac{k_{p,20} - k_{p,02} - 2 \cdot k_{p,00}}{1 + \frac{k_{p,00}}{k_{p,22}}} \quad (3)$$

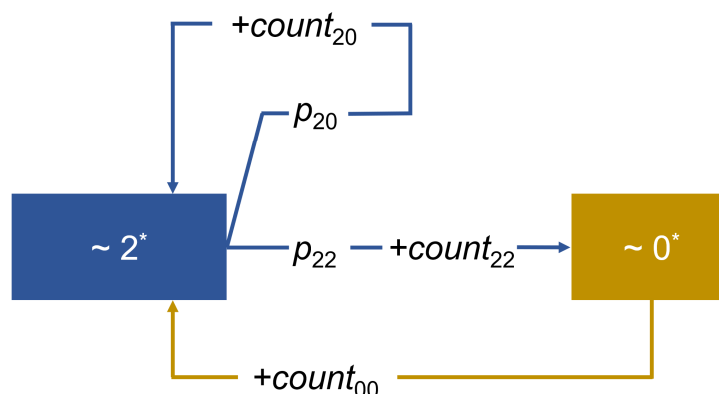
As already discussed, based on Scheme 2, tail-to-head growth does not occur, thus the coefficient $k_{p,02}$ is equal to 0, and Equation (3) simplifies accordingly. Furthermore, Siegmann et al. described the overall propagation rate coefficient of VDF for polymerizations in solution with supercritical carbon dioxide by Equation (4) over a wide range of temperatures and pressures [25].

$$\ln k_{p,\text{app}} = \ln A - \frac{E_a}{R \cdot T} - \frac{\Delta V^\ddagger \cdot p}{R \cdot T} \quad (4)$$

with p introduced in bar and T in K. A represents the pre-exponential factor, E_a denotes the activation energy, T signifies the temperature, p stands for pressure, and R represents the universal gas constant. For VDF, the activation energy is found to be $30.2 \text{ kJ} \cdot \text{mol}^{-1}$, the activation volume is $-22.7 \text{ cm}^3 \cdot \text{mol}^{-1}$, and the pre-exponential factor is $4.66 \cdot 10^8 \text{ L} \cdot \text{mol}^{-1} \cdot \text{s}^{-1}$ [25].

For calculating the defect fraction using the individual propagation rate coefficients $k_{p,00}$, $k_{p,20}$, and $k_{p,22}$, a simple Monte Carlo simulation of chain growth was implemented in the Python programming language. An illustrated representation of the simulation is shown in Scheme 4. The corresponding Python script for the Monte Carlo simulations is provided in the Supporting Information as file `pvdF-defect.txt`. The addition of

10^7 monomer units was recorded in the simulation. As a result, the program outputs the temperature-dependent values of $k_{p,app}$ and the fraction of defects.



Scheme 4. Scheme of polymer chain propagation simulation.

The simulation starts with a growing chain end “ $\sim 2^*$ ”. The probability of regular growth p_{20} can be determined using the coefficients $k_{p,20}$ and $k_{p,22}$ according to Equation (5).

$$p_{20} = \frac{(k_{p,20}/k_{p,22})}{(k_{p,20}/k_{p,22}) + 1} \quad (5)$$

Using a random number r ($0 \leq r \leq 1$), it is decided whether regular or irregular growth occurs at the chain end. If the random number is less than or equal to p_{20} , regular growth occurs, and the counter $count_{20}$ is incremented by 1. After this growth step, the chain end remains unchanged as “ $\sim 2^*$ ”. The probability p_{22} is $1 - p_{20}$. Therefore, if the random number r is $r > p_{20}$, the pathway of irregular growth is selected. The chain end changes to “ $\sim 0^*$ ”, and the defect structure counter $count_{22}$ increases by 1. Since instantaneous self-healing occurs, the chain end switches back to “ $\sim 2^*$ ” in the subsequent propagation step, and the counter $count_{00}$ is incremented by 1. For the simulation, 10^6 addition steps were performed, and the defect fraction was calculated from the counters according to Equation (6).

$$defect\ fraction_{sim} = \frac{count_{22}}{count_{22} + count_{00} + count_{20}} \times 100\% \quad (6)$$

The goal of the optimization is to achieve a good match of the defect fraction with experimental data. Therefore, the sum of squared differences is minimized while varying the coefficients $k_{p,00}$, $k_{p,20}$, and $k_{p,22}$. A constraint is that the $k_{p,app}$ calculated using the determined individual coefficients matches the experimental data within the experimental error limits. For this purpose, a stochastic Metropolis–Hastings algorithm was used, as described in detail by Feuerpfeil et al. [31]. The result of the optimization is presented in Table 1. The activation energy of the regular monomer addition, $E_{a,20} = 25.5 \text{ kJ}\cdot\text{mol}^{-1}$, is significantly lower than for the inverse propagation, $E_{a,22} = 30.7 \text{ kJ}\cdot\text{mol}^{-1}$, which explains the increase in defect structures at higher temperatures. The temperature dependence of the self-healing reaction is the most pronounced, as indicated by the activation energy, $E_{a,00}$, of $35.4 \text{ kJ}\cdot\text{mol}^{-1}$. The pre-exponential factor of the inverse propagation reaction is the lowest, which is in line with the small fraction of defect structures. For example, the kinetic coefficients $k_{p,20}$, $k_{p,22}$, and $k_{p,00}$ calculated for $45 \text{ }^\circ\text{C}$ with the Arrhenius parameters according to $k = A \cdot \exp(-E_a/RT)$ are $12,900 \text{ L}\cdot\text{mol}^{-1}\cdot\text{s}^{-1}$, $592 \text{ L}\cdot\text{mol}^{-1}\cdot\text{s}^{-1}$, and $5430 \text{ L}\cdot\text{mol}^{-1}\cdot\text{s}^{-1}$, respectively. As expected, the predominantly occurring regular head-to-tail addition is the fastest reaction, and the associated $k_{p,20}$ is higher by a factor of 22 than the kinetic coefficient $k_{p,22}$ for defect growth. The self-healing reaction coefficient is a factor of two lower than for the regular chain propagation. At $90 \text{ }^\circ\text{C}$ the differences between $k_{p,20}$

and $k_{p,22}$ are slightly lower due to the higher activation energy of $k_{p,22}$, with $k_{p,20}$ being 17 times higher than $k_{p,22}$.

Table 1. Determined activation energies and pre-exponential factors.

A_{20}	A_{22}	A_{00}	$E_{a,20}$	$E_{a,22}$	$E_{a,00}$
$\text{L}\cdot\text{mol}^{-1}\cdot\text{s}^{-1}$			$\text{kJ}\cdot\text{mol}^{-1}$		
1.99×10^8	6.50×10^7	3.52×10^9	25.5	30.7	35.4

In Table 2 and Figure 3, a very good agreement between the calculated fraction of defect structures and the experimental data are shown. Table 2 also demonstrates that the constraint regarding $k_{p,app}$ is met. A linear dependence of the fraction of defect structures with increasing reaction temperature is observed, as shown in Figure 3. The fraction of defect structures determined from the NMR spectra is in good agreement with the literature reports. For example, Guerre et al. reported a percentage of 4.1% for the defect structures of PVDF from RAFT (reversible addition fragmentation transfer) polymerizations at 75 °C, resulting in polymers with rather low average molar masses, M_n , of, at most, 13,800 $\text{g}\cdot\text{mol}^{-1}$ [16]. It was pointed out that the fraction of defects increases with conversion and polymer molar mass. In contrast to the literature data, the results in Table 2 were obtained for polymers from free-radical polymerizations with significantly higher molar masses, e.g., with M_n being higher than 40,000 $\text{g}\cdot\text{mol}^{-1}$. Therefore, the slightly higher defect fractions in Table 2 are due to the higher PVDF molar mass.

Table 2. Experimentally determined defect contents and calculated average growth rate coefficients $k_{p,app}$ at different polymerization temperatures.

$T/^\circ\text{C}$	$defect\ fraction_{exp}/\%$	$defect\ fraction_{sim}/\%$	$k_{p,app,exp}/\text{L}\cdot\text{mol}^{-1}\cdot\text{s}^{-1}$	$k_{p,app,sim}/\text{L}\cdot\text{mol}^{-1}\cdot\text{s}^{-1}$
45	4.2	4.2	11,200	12,700
60	4.5	4.5	20,000	19,900
65	4.7	4.6	23,300	23,000
75	4.8	4.8	30,900	30,100
90	5.2	5.2	46,000	43,800

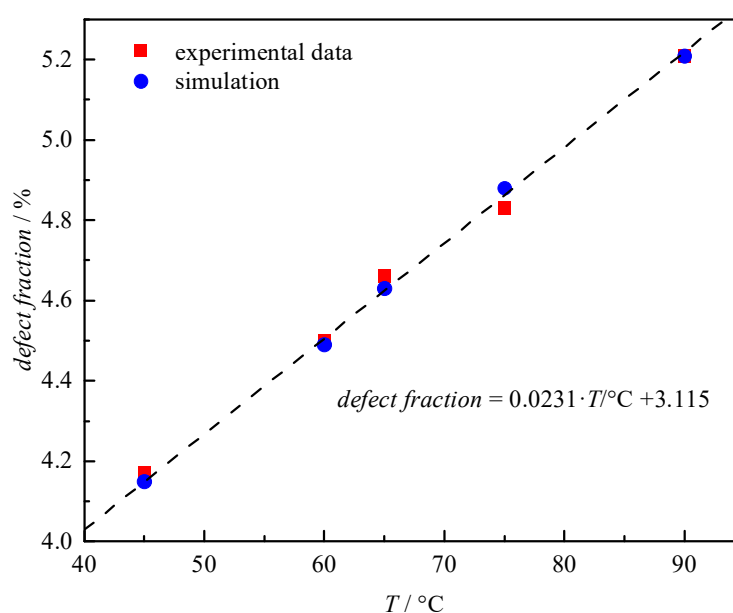


Figure 3. Experimental and simulated defect fraction of PVDF as a function of temperature.

Moreover, it is important to note that the largely varying activation energies of the various propagation reactions are important for the data evaluation. The VDF system is not suited for a description of the defect structures based on ratios of propagation rate coefficients, e.g., comparable to the previously reported use of reactivity ratios in the case of vinyl acetate polymerizations [32].

3. Materials and Methods

VDF is polymerized via pulsed laser-induced polymerization (PLP) in homogeneous phase with supercritical CO₂ as the reaction medium in an optical high-pressure cell [33]. The reaction mixture consisting of VDF (99%, provided by 3M/Dyneon, Burgkirchen an der Alz, Germany) and carbon dioxide (CO₂, ≥99% by volume, Westfalen AG, Münster, Germany), and the photoinitiator 2,2-dimethoxy-2-phenylacetophenone (DMPA, 99%, Acros Organics, Geel, Belgium) is prepared and transferred into the optical high-pressure cell as reported previously [25]. PLP experiments are carried out at temperatures of 45 °C, 60 °C, 65 °C, 75 °C, and 90 °C at a pressure of 1050 bar. An excimer laser (ExiStar XS 500, Coherent, Santa Clara, CA, USA) operated at a wavelength of 351 nm with a pulse repetition rate adjustable between 1 and 500 Hz is used. Details of the pulsed-laser-initiated polymerizations in solution with supercritical CO₂ and the measurements of the molar mass distributions using size-exclusion chromatography are provided elsewhere [25,26]. As solvents for the NMR measurements with a Bruker AVANCE 400 MHz spectrometer, deuterated N,N-dimethylformamide (DMF-d₇, 99.5%, Deutero GmbH, Kastellaun, Germany) and acetone-d₆ (99.8%, Deutero GmbH) are used.

It is important to note that, in the case of the PLP of VDF in solution with supercritical CO₂, only little variation in temperature below 1 °C may be achieved due to the design of the reaction cell [28]. Moreover, applying the laser pulses in several sequences, the presence of supercritical CO₂ as a solvent, and stopping the reaction at a monomer conversion below 5%, all contribute to good temperature control, too. Further, the presence of CO₂ does not affect the propagation rate coefficients [34,35].

4. Conclusions

The polymerization temperature has a significant impact on the proportion of defect structures in PVDF, and thus, on the thermal and mechanical properties of the polymer. For this reason, it is important to precisely control the reaction temperature during synthesis. Based on ¹⁹F-NMR spectroscopy, the fraction of defect structures was calculated, which is well-expressed by a linear relation. In addition, a Monte Carlo simulation was performed. The fraction of defect structures from the simulation matches very well with the experimental data, and the constraint, which is the good agreement of $k_{p,app,sim}$ and $k_{p,app,exp}$, is well maintained. The individual propagation rate coefficients $k_{p,20}$, $k_{p,22}$, and $k_{p,00}$ are determined as a function of temperature, with the associated activation energies being largely different. Particularly important is the activation energy of 30.7 kJ·mol⁻¹ for the inverse propagation reaction, whereas a significantly lower value of 25.5 kJ·mol⁻¹ is derived for the regular propagation reaction. The individual rate coefficients with temperature dependence are required to assist in tailoring the fraction of defect structures in the product using simulations.

Supplementary Materials: The following supporting information can be downloaded at: <https://www.mdpi.com/article/10.3390/molecules29071551/s1>, pvdf-defect.txt.

Author Contributions: Conceptualization, S.B.; formal analysis, J.S.; writing—original draft, J.S. and M.D.; writing—review and editing, S.B.; visualization, J.S.; simulation, M.D.; project administration, S.B. All authors have read and agreed to the published version of the manuscript.

Funding: This research received no external funding.

Institutional Review Board Statement: Not applicable.

Informed Consent Statement: Not applicable.

Data Availability Statement: Data are contained within the article.

Conflicts of Interest: The authors declare no conflict of interest.

References

1. Gardiner, J. Fluoropolymers: Origin, Production, and Industrial and Commercial Applications. *Aust. J. Chem.* **2015**, *68*, 13–22. [[CrossRef](#)]
2. Ameduri, B. Fluoropolymers: The right material for the right application. *Chem. Eur. J.* **2018**, *24*, 18830–18841. [[CrossRef](#)]
3. Liu, F.; Hashim, N.A.; Liu, Y.; Abed, M.R.M.; Li, K. Progress in the production and modification of PVDF membranes. *J. Membr. Sci.* **2011**, *375*, 1–27. [[CrossRef](#)]
4. Marcus, M.A. Ferroelectric polymers and their applications. *Ferroelectrics* **1982**, *40*, 29–41. [[CrossRef](#)]
5. Martins, P.; Lopes, A.C.; Lanceros-Mendez, S. Electroactive phases of poly(vinylidene fluoride): Determination, processing and applications. *Prog. Polym. Sci.* **2014**, *39*, 683–706. [[CrossRef](#)]
6. Dillon, D.R.; Tenneti, K.K.; Li, C.Y.; Ko, F.K.; Sics, I.; Hsiao, B.S. On the structure and morphology of polyvinylidene fluoride-nanoclay nanocomposites. *Polymer* **2006**, *47*, 1678–1688. [[CrossRef](#)]
7. Ameduri, B. From Vinylidene Fluoride (VDF) to the Applications of VDF-Containing Polymers and Copolymers: Recent Developments and Future Trends. *Chem. Rev.* **2009**, *109*, 6632–6686. [[CrossRef](#)]
8. Soulestin, T.; Ladmiraal, V.; Dos Santos, F.D.; Ameduri, B. Vinylidene fluoride- and trifluoroethylene-containing fluorinated electroactive copolymers. How does chemistry impact properties? *Prog. Polym. Sci.* **2017**, *72*, 16–60. [[CrossRef](#)]
9. Pladis, P.; Alexopoulos, A.H.; Kiparissides, C. Mathematical Modeling and Simulation of Vinylidene Fluoride Emulsion Polymerization. *Ind. Eng. Chem. Res.* **2014**, *53*, 7352–7364. [[CrossRef](#)]
10. Brandl, F.; Beuermann, S. Semibatch Emulsion Polymerization of Vinylidene fluoride. *Chem. Ing. Technol.* **2018**, *90*, 372–379. [[CrossRef](#)]
11. Boyer, C.; Valade, D.; Sauguet, L.; Ameduri, B.; Boutevin, B. Iodine Transfer Polymerization (IPT) of Vinylidene Fluoride (VDF). Influence of the Defect of VDF Chaining on the Control of ITP. *Macromolecules* **2005**, *38*, 10353–10362. [[CrossRef](#)]
12. Modena, S.; Pianca, M.; Tato, M.; Moggi, G. Radical Telomerization of Vinylidene Fluoride in the Presence of 1,2-Dibromotetrafluoroethane. *J. Fluor. Chem.* **1989**, *43*, 15–25. [[CrossRef](#)]
13. Maiti, P.; Nandi, A.K. Influence of Chain Structure on the Miscibility of Poly(vinylidene fluoride) with Poly(methyl acrylate). *Macromolecules* **1995**, *28*, 8511–8516. [[CrossRef](#)]
14. Durand, N.; Ameduri, B.; Takashima, K.; Ishida, K.; Horie, S.; Ueda, Y. Vinylidene fluoride telomers for piezoelectric devices. *Polym. J.* **2011**, *43*, 171–179. [[CrossRef](#)]
15. Lovinger, A.J.; Davis, D.D.; Cais, R.E.; Kometani, J.M. The role of molecular defects on the structure and phase transitions of poly(vinylidene fluoride). *Polymer* **1987**, *28*, 617–626. [[CrossRef](#)]
16. Vohlidal, J.; Graeff, C.F.O.; Hiorns, R.C.; Jones, R.G.; Luscombe, C.; Schué, F.; Stingelin, N.; Walter, M.G. Glossary of terms relating to electronic, photonic and magnetic properties of polymers (IUPAC Recommendations 2021). *Pure Appl. Chem.* **2022**, *94*, 15–69. [[CrossRef](#)]
17. Guerre, M.; Rahaman, S.M.W.; Ameduri, B.; Poli, R.; Ladmiraal, V. Limits of Vinylidene Fluoride RAFT Polymerization. *Macromolecules* **2016**, *49*, 5386–5396. [[CrossRef](#)]
18. Balague, J.; Ameduri, B.; Boutevin, B.; Caporiccio, G. Synthesis of fluorinated telomers. Part 1. Telomerization of vinylidene fluoride with perfluoroalkyl iodides. *J. Fluor. Chem.* **1995**, *70*, 215–223. [[CrossRef](#)]
19. Russo, S.; Behari, K.; Chengji, S.; Pianca, M.; Barchiesi, E.; Moggi, G. Synthesis and microstructural characterization of low-molar-mass poly(vinylidene fluoride). *Polymer* **1993**, *34*, 4777–4781. [[CrossRef](#)]
20. Guiot, J.; Ameduri, B.; Boutevin, B. Radical Homopolymerization of Vinylidene Fluoride Initiated by tert-Butyl Peroxypivalate. Investigation of the Microstructure by ^{19}F and ^1H NMR Spectroscopies and Mechanisms. *Macromolecules* **2002**, *35*, 8694–8707. [[CrossRef](#)]
21. Ameduri, B.; Ladaviere, C.; Delolme, F.; Boutevin, B. First MALDI-TOF Mass Spectrometry of Vinylidene Fluoride Telomers Endowed with Low Defect Chaining. *Macromolecules* **2004**, *37*, 7602–7609. [[CrossRef](#)]
22. Patil, Y.; Zhao, J.; Ameduri, B.; Rastogi, S. Tailoring Electroactive β - and γ -Phases via Synthesis in the Nascent Poly(vinylidene fluoride) Homopolymers. *Macromolecules* **2024**, *57*, 616–627. [[CrossRef](#)]
23. Giannetti, E. Semi-crystalline fluorinated polymers. *Polym. Int.* **2001**, *50*, 10–26. [[CrossRef](#)]
24. Timmerman, R. The Predominant Reaction of Some Fluorinated Polymers to Ionizing Radiation. *J. Appl. Polym. Sci.* **1962**, *22*, 456–460. [[CrossRef](#)]
25. Siegmann, R.; Drache, M.; Beuermann, S. Propagation Rate Coefficients for Vinylidene Fluoride Homopolymerizations. *Macromolecules* **2013**, *46*, 9507–9514. [[CrossRef](#)]
26. Schäfer, T. Kinetische Untersuchungen und PREDICI Modellierung der Puls-laser-induzierten Hochdruckpolymerisation von Vinylidenfluorid in Überkritischem Kohlendioxid. Ph.D. Thesis, TU Clausthal, Clausthal-Zellerfeld, Germany, 2017.
27. Olaj, O.F.; Bitai, I.; Hinkelmann, F. The laser-flash-initiated polymerization as a tool of evaluating (individual) kinetic constants of free-radical polymerization, The direct determination of the rate constant of chain propagation. *Makromol. Chem.* **1987**, *188*, 1689–1702. [[CrossRef](#)]

28. Beuermann, S.; Buback, M. Rate coefficients of free-radical polymerization deduced from pulsed laser experiments. *Prog. Polym. Sci.* **2002**, *27*, 191–254. [[CrossRef](#)]
29. Twum, E.B.; Li, X.; McCord, E.F.; Fox, P.A.; Lyons, D.F.; Rinaldi, P.L. 2D-NMR Studies of Polyvinylidene Fluoride. In *Fluorine Containing Polymers: Advances in Fluorine-Containing Polymers*; Smith, D.W., Iacono, S.T., Kettwich, S.C., Boday, D.J., Eds.; American Chemical Society: Washington, DC, USA, 2012; pp. 187–213. [[CrossRef](#)]
30. Monyatsi, O.; Nikitin, A.N.; Hutchinson, R.A. Effect of Head-To-Head Addition on Vinyl Acetate Propagation Kinetics in Radical Polymerization. *Macromolecules* **2014**, *47*, 8145–8153. [[CrossRef](#)]
31. Feuerpfeil, A.; Drache, M.; Jantke, L.-A.; Melchin, T.; Rodriguez-Fernandez, J.; Beuermann, S. Modeling Semi-Batch Vinyl Acetate Polymerization Processes. *Ind. Eng. Chem. Res.* **2021**, *60*, 18256–18267. [[CrossRef](#)]
32. Drache, M.; Stehle, M.; Mätzig, J.; Brandl, K.; Jungbluth, M.; Namyslo, J.C.; Schmidt, A.; Beuermann, S. Identification of β scission products from free radical polymerizations of butyl acrylate at high temperature. *Polym. Chem.* **2019**, *10*, 1956. [[CrossRef](#)]
33. van Herk, A.M.; Manders, L.G.; Canelas, D.A.; Quadir, M.A.; DeSimone, J.M. Propagation rate coefficients of styrene and methyl methacrylate in supercritical CO₂. *Macromolecules* **1997**, *30*, 4780–4782. [[CrossRef](#)]
34. Beuermann, S.; Buback, M.; Isemer, C.; Lacik, I.; Wahl, A. Pressure and Temperature Dependence of the Propagation Rate Coefficient of Free-Radical Styrene Polymerization in Supercritical Carbon Dioxide. *Macromolecules* **2002**, *35*, 3866–3869. [[CrossRef](#)]
35. Beuermann, S.; Buback, M.; Schmaltz, C.; Kutcha, F.-D. Determination of free-radical propagation rate coefficients for methyl methacrylate and butyl acrylate homopolymerizations in fluid CO₂. *Macromol. Chem. Phys.* **1998**, *199*, 1209–1216. [[CrossRef](#)]

Disclaimer/Publisher's Note: The statements, opinions and data contained in all publications are solely those of the individual author(s) and contributor(s) and not of MDPI and/or the editor(s). MDPI and/or the editor(s) disclaim responsibility for any injury to people or property resulting from any ideas, methods, instructions or products referred to in the content.